SAND2017-6332C

SIMULATING RESIDUAL STRESSES IN SIMPLE MULTI-MATERIAL COMPOSITE STRUCTURES

Alexander A. Hanson[1], Stacy M. Nelson[1], Alyssa J. Skulborstad[1], Brian T. Werner[1], Timothy M. Briggs[1]

[1]Sandia National Laboratories
Livermore, CA 94551-0969

ABSTRACT

Process induced residual stresses commonly occur in composite structures composed of dissimilar materials. These residual stresses form due to differences in the composite materials' coefficients of thermal expansion as well as the shrinkage upon cure exhibited by most thermoset polymer matrix materials. Depending upon the specific geometric details of the composite structure and the materials' curing parameters, it is possible that these residual stresses can result in interlaminar delamination and fracture within the composite as well as plastic deformation in the structure's metallic materials. Therefore, the consideration of potential residual stresses is important when designing composite parts and their manufacturing processes. However, the experimental determination of residual stresses in prototype parts can be prohibitive, both in terms of financial and temporal costs. As an alternative to physical measurement, it is possible for computational tools to be used to quantify potential residual stresses in composite prototype parts. A simplified method for simulating residual stresses was previously validated with two simple bi-material structures composed of aluminum and a carbon fiber/epoxy resin composite. Therefore, the objective of this study is to further validate the simplified method for simulating residual stresses for different composites and more complex structures. The simplified method accounts for both the coefficient of thermal expansion mismatch and polymer shrinkage through the calibration to an experimentally-determined stress-free temperature. This was implemented in Sandia National Laboratories' solid mechanics code, SIERRA, to model split rings with temperature independent and dependent material models. The split rings are comprised of two materials: aluminum with either a carbon fiber/epoxy resin composite or a glass fiber/epoxy resin composite. Concurrent with the computational efforts, structures similar to those modeled are fabricated and the residual stresses are quantified through the measurement of deformations. The simulations' results are compared to the experimentally observed behaviors for model validation. The results of the comparisons indicate that the proposed finite element modeling approach is capable of accurately simulating the formation of residual stresses in composite structures and a temperature independent material model is adequate within the composite's glassy region.

Sandia National Laboratories is a multimission laboratory managed and operated by National Technology and Engineering Solutions of Sandia, LLC, a wholly owned subsidiary of Honeywell International, Inc., for the U.S. Department of Energy's National Nuclear Security Administration under contract DE-NA0003525.

1. INTRODUCTION

Residual stresses in composite structures developed during the curing process, especially at the interface with another material, can lead to delamination or failure of the composite. Experiments can be done to determine the residual stress of a component; however, these are costly and difficult depending on the geometry of the component. As an alternative, validated computer simulations can be used to predict the residual stress and subsequent failure of a component. This represents a potential cost and time savings in the design process of components including composite materials.

There is a wide range of models than can be used to predict residual stresses in structures containing composite materials. The complexity of these models range from the simplest given by the analytical solution of Timoshenko to full process modeling that includes temperature dependence of materials and cure kinetics [1-7]. While the analytical equation presented by Timoshenko works reasonably well, it is limited in its application to one-dimensional, uniform and constant materials, and small strain [1]. Jumbo et. al. converts Timoshenko's equation to two dimensions by replacing the elastic moduli with the corresponding bi-axial moduli; however, the equations are still limited to uniform materials and small strain [2]. Neither application can account for polymer shrinkage – a non-negligible factor in determining residual stresses in thermoset polymers. Since cure kinetics of a thermoset polymer composite can be quite impactful to the residual stress seen in a composite, White and Hahn developed a process modeling approach for composites [3, 4]. The process model follows the temperature history of the composite and follows the transition of a composite from its uncured to cured state. Expanding upon the principles of process modeling of composites, Tavakol et. al. developed a three-dimensional coupled thermomechanical process model that determines the mechanical properties on an element based on the temperature and cure kinetics (i.e. degree of cure) [5]. A similar process was also used by Volk et. al. to predict the residual stresses in various geometries [6, 7]. Full process modeling of thermoset polymer composites often requires many input parameters to fully define the cure kinetics, thermal, and mechanical properties, which may be difficult or costly to obtain.

In order to reduce the number of parameters, a simplified approach may be used to predict residual stresses, at the cost of no longer containing the necessary information to predict more complex phenomena, such as creep. The simplified approach uses one experimentally defined parameter, the stress free temperature, to account for the effects of cure kinetics and polymer shrinkage and accounts for the remainder of the residual stress with coefficients of thermal expansion. Jumbo et. al. applied this approach to bi-material strips comprised of metals and neat resins (both isotropic materials) and Hanson et. al. further applied the method to bi-material geometries with orthotropic composites [2, 8]. Both studies showed acceptable results when compared to the experiments and Jumbo et. al. concluded that temperature dependent material properties and the inclusion of geometric non-linearity was necessary to capture the bending of the bi-material strips.

Continuing the validation of the simplified approach with orthotropic composites, the objective of this study is to determine effectiveness of the approach with other composite materials, orientations, and temperature dependent material properties. Specifically, a carbon fiber/epoxy and aluminum split ring will be investigated with two different ply orientations as well as a glass fiber/epoxy and aluminum split ring. Furthermore, a temperature dependent material model will be compared to a temperature independent material model for each investigation. Concurrent with

simulations, experiments over a range of temperatures are conducted to continue to evaluate the viability of the simplified approach to modeling residual stresses.

2. EXPERIMENTATION

2.1 Geometry and Materials

Two composite materials were considered for this investigation: carbon fiber/epoxy and glass fiber/epoxy. Both materials consisted of an 8-harness satin (8HS) weave of AS4C carbon fibers or 7781 e-glass fibers and preimpregnated with TCR 3362 resin. Laminates were laid by hand from pre-cut ply kits made using a CNC ply cutter to control geometry and fiber orientation and cured in the form of a bi-material cylinder using a standard autoclave process with a 4-hour hold at 176.7 °C.

The aluminum of the cylinder was fabricated from a 6063-T6 number 4, schedule 10 pipe. The inner diameter (108.20 mm) was maintained and the outer diameter was machined to 112.27 mm ± 2.54 mm, resulting in a nominal thickness of 2.03 mm. Post-machining measurements were taken at eight points about the circumference, showing the average thickness to be 1.91 mm for the aluminum used with the carbon fiber composite and 1.86 mm for the glass fiber composite.

The composite stack sequence comprised of four plies for the carbon fiber composite and six plies for the glass fiber composite, both laid up symmetrically with respect to the mid plane. A total of three composite/orientation combinations were fabricated: carbon fiber with the warp direction orientated about the circumference, glass fiber with the warp direction orientated about the circumference, and carbon fiber with the warp direction skewed 45°. Measurements of the by-material cylinder's total thickness were taken post cure, giving an average thickness of 3.46 mm and 3.34 mm (1.55 mm and 1.49 mm of composite) for the carbon fiber and glass fiber cylinders, respectively.

The composite materials were co-bonded to an aluminum surface that had been lightly abraded, acetone cleaned, and primed. Previous bi-material experiments that excluded priming the aluminum surface resulted in de-bonding of the materials over time due to the residual stresses. The bi-material cylinders were cured using standard practices of caul plates (in this case, comprised of silicon in order to wrap around the cylinder), release films, bleeder, and edge string bleeder were employed to adequately consolidate and devolatilize the laminate during cure. Edge embedded thermocouples were actively used to monitor and drive the cure of the laminate. A typical in-process view of the cylinder configuration can be seen in Figure 1.

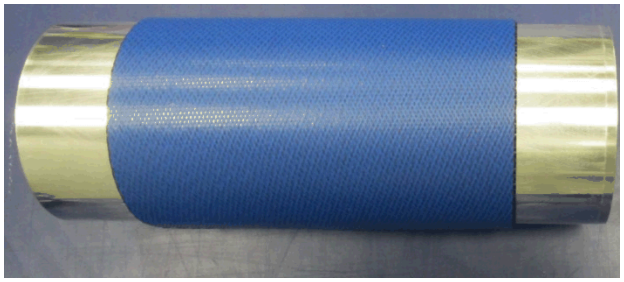

Figure 1. In-process layup of the cylinder.

2.2 Manufacturing Process

The cylinder was machined in order to produce six 25.4 mm wide rings that then had an approximately 32.5 mm (35°) wide sector removed, resulting in a split ring geometry the visually shows the effects of residual stresses. Prior to machining, scribe lines were etched into the composite and were measured: 47.93 mm, 49.43 mm, and 49.45 mm wide for the carbon fiber composite (no skew), carbon fiber composite (45° skew), and for the glass fiber composite, respectively. The scribe lines allow for the estimation of the stress free temperature (the temperature where the scribe lines return to their pre-machined width).

The sector removed from each ring to create the split was approximately 35° or 32.5 mm in length, thus allowing the ring to close in on itself due to the residual stress at the interface. The details of the split ring processing can be seen in Figure 2 and Figure 3 shows the three variations that were investigated.

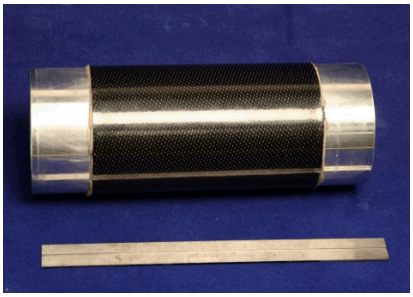

Consolidated bi-material cylinder

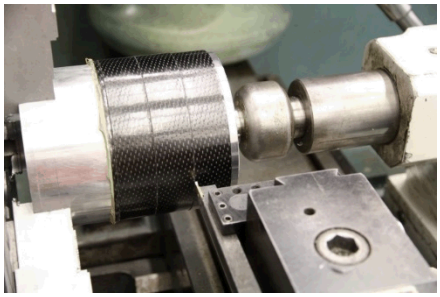

Lathe cutting cylinder down into rings

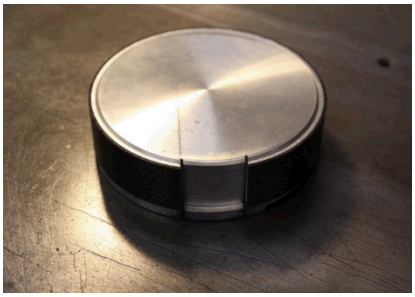

Ring has been split by removing 35° sector

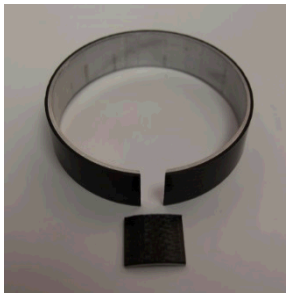

Ring closes in on itself at room temperature due to residual stresses

Figure 2. The bi-material cylinder is processed into split rings to observe the gap width as a function of temperature.

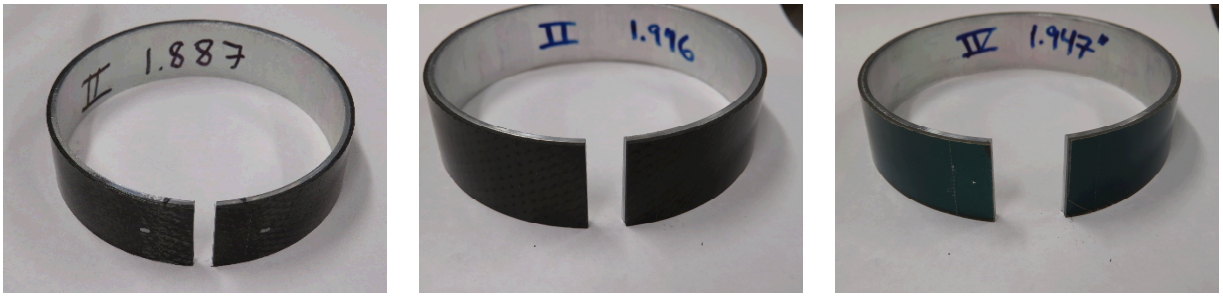

Figure 3. Bi-material cylinders at room temperature: carbon fiber composite – no skew (left), carbon fiber composite – 45° skew (center), and glass fiber composite – no skew (right).

2.3 Experimental Procedure

By using a symmetric stack sequence for the composite in both geometries, any thermal residual stress would, in most part, be solely due to the polymer shrinkage and the coefficient of thermal expansion (CTE) mismatch between the aluminum and composite material. The approach in this experimental phase of the investigation was to observe and measure the width of the scribe lines as a function of temperature.

The temperature was increased from room temperature (approximately 25 °C) to 170 °C at a rate of 0.5 °C per minute and then decreased back to room temperature at the same rate (Figure 4). A faster rate would produce large temperature differences between the aluminum and composite due to their differing thermal properties and would result in a hysteresis loop over the heatup and cooldown cycle. Even with the slow rate to minimize the temperature difference, during the heatup phase, temperature differences between could exceed 5 °C, whereas the cooldown minimized the temperature differences to be less than 1 °C, as shown in Figure 4. Therefore, the results of the cooldown were used to compare to the simulations.

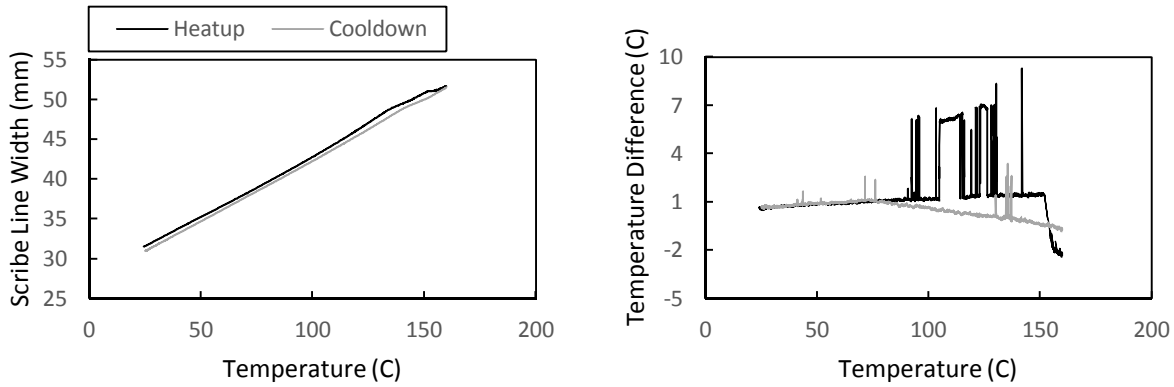

Figure 4. Heatup and cooldown scribe line widths (left) and aluminim-composite temperature difference (right).

The scribe lines were measured throughout the heating and cooling process using an extensometer attached to the split ring at the scribe lines, as shown in Figure 5.

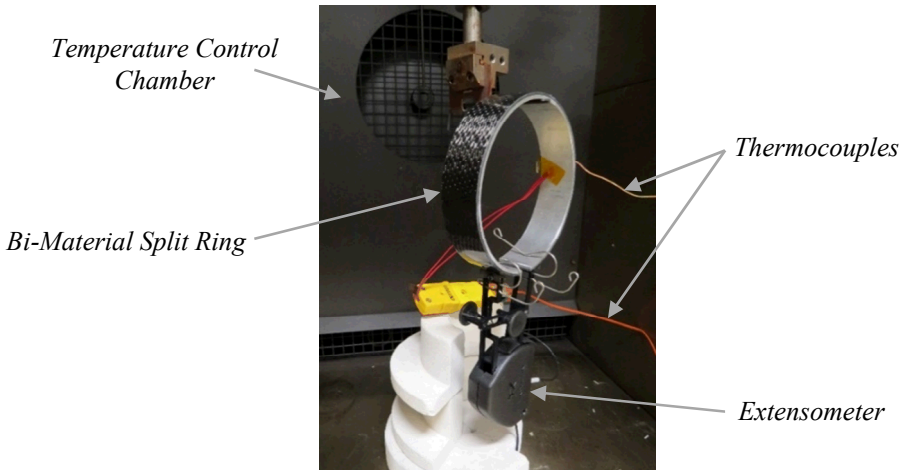

Figure 5. Experimental setup.

3. SIMULATION

3.1 Simulation Process

During the curing process, the composite will volumetrically shrink and impart a residual stress in the component. As a bi-material geometry begins to cool, the mismatched coefficients of thermal expansion will eventually nullify the residual stress induced by the polymer shrinkage at the stress free temperature resulting in a stress free temperature that is lower than the cure temperature [9]. Therefore, heating a bi-materials geometry to the experimentally determined stress free temperature instead of the cure temperature allows for the effect of polymer shrinkage to be indirectly incorporated (Figure 6). Based on this, the simulation reduces the analysis cure cycle to a simple ramp up to the stress free temperature and a ramp back to room temperature. In total, the simulation consists of three steps with a fourth step to match the thermal excursion of the experiments.

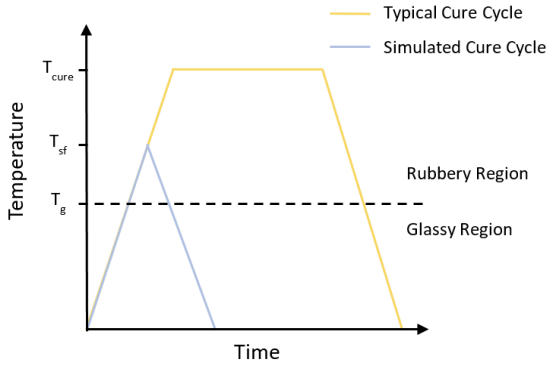

Figure 6. Comparison of the simulated cure cycle (Steps 1 and 2) and a typical cure cycle.

The first step of the simulation isothermally heats the split ring from room temperature to the stress free temperature (144.1 °C and 144.7 °C for the carbon and glass fiber composite split rings, respectively) where the simulation is then stopped. During this step the composite is uncured and is modeled as a compliant, incompressible material such that it does not constrain the thermal expansion of the aluminum. Stopping the analysis at the stress free temperature allows the cured composite material to be activated at a known stress free state for the next analysis step while the aluminum maintains its size and shape. Furthermore, it allows for the deactivation of the un-cured, compliant material properties and the activation of the cured material properties in the subsequent analysis step. This simplifies the simulation of the curing process by simulating the composite material property transformation as a step change.

The second step performs the deactivation of the un-cured composite materials and the activation of the cured composite materials before cooling the geometries back to room temperature. At the onset of the second step the cured composite and aluminum are activated in a stress free state by only transferring the thermal strains and temperatures from the initial analysis step. As the cylinder begins to cool, residual stresses will begin to develop due to the dissimilar coefficients of thermal expansion.

The residual stresses remain visibly undetectable until the third analysis step where the sector is removed from the cylinder to create a split ring and spring-in occurs. The third analysis step simply solves for static equilibrium after removing the sector from the model.

3.2 Analysis Software

The Sandia National Laboratories' developed implicit finite element code SIERRA Adagio was used to solve the simulations [10]. Adagio is a Lagrangian, three-dimensional implicit code for the finite element analysis of solid structures, which is suitable for the quasistatic nature of these analyses.

3.3 Element Formulation

All simulations were solved using eight-noded hexahedral elements using the uniform gradient (reduced integration) formulation that is default to SIERRA. The strain incrementation was set to be strongly objective rather than the default, midpoint incrementation. Strongly objective incrementations, while computationally more expensive, gives better accuracy for large time steps and deformations involving both rotation and stretch.

3.4 Materials

3.4.1 Material Models

The specification of three materials is needed to simulate the curing process of the bi-material split ring: aluminum, un-cured composite, and cured composite.

The aluminum was modeled using Sierra Adagio's elastic material model for temperature independent properties and the thermoelastic material model for the temperature dependent properties. Both models produce linear elastic behavior and require the specification of the density, Young's Modulus, and Poisson's ratio [10]. The thermoelastic model allows the Young's Modulus and Poisson's ratio to be specified as functions (of temperature) whereas they must be constant in the elastic model. These models are sufficient as no yielding or failure is expected in to occur in the aluminum, nor has it occurred in previous experiments [8].

Both the un-cured and cured composites were modeled using homogenized material properties and Sierra Adagio's elastic orthotropic material model [10]. The regular nine independent constants (Young's modulus, shear modulus, and Poisson's ratios in the three material directions) are needed to fully define the elastic orthotropic model. Furthermore, the material model calls for the density and coordinate rotations to properly align the material coordinate system.

3.4.2 Un-cured Composite Material Properties

In its un-cured state, the epoxy matrix of the composite materials has the ability to flow and will not restrict the thermal expansion of the aluminum. As such, the un-cured composite was modeled as a compliant and incompressible elastic material using Sierra Adagio's elastic orthotropic model. Using a perfectly compliant and incompressible material ($E = 0$ Pa and $\nu = 0.5$) resulted in convergence problems that were resolved by using properties sufficiently similar, as shown in Table 1.

Additionally, the un-cured composite was given the same coefficient of thermal expansion (CTE) as the aluminum in the in-plane material directions to prevent any restriction of the aluminum due to differences in thermal strains. The cured composite CTE was specified for the material direction normal to the plies (out-of-plane or the 33 direction) in order to maintain zero thermal strain at room temperature for the thickness of the composite.

The mechanical properties of the un-cured composite remain constant for both the temperature dependent and independent models with the temperature only differing from the temperature independent model by the use of aluminum's temperature dependent thermal strains.

Table 1. Un-Cured Composite Material Properties (Elastic Material Model).

Density (kg/m^3)	1,600
Young's Modulus (MPa)	1
Poisson's Ratio	0.4999

3.4.3 Temperature Dependent Properties

A temperature dependent Young's modulus for aluminum is given by Table TM-2 of the ASME Boiler and Pressure Vessel Code (BPVC), as shown in Table 2 [11].

The mechanical properties of the cured composite materials were determined through experiments for E_{11}, E_{22}, ν_{12}, and G_{12} at 54 °C, 25 °C, and 71°C. The remaining mechanical properties were determined through other experiments at room temperature (25 °C) or through micromechanical modeling and then given temperature dependence by scaling the temperature dependence of G_{12}. For temperatures above 71 °C, the temperature dependence was extrapolated.

For the carbon fiber composite, the mechanical properties dominated by the fibers (E_{11}, E_{22}, and ν_{12}) showed little or no temperature dependence and were held constant at their room temperature values. The values for ν_{13} and ν_{23} were also held constant for both composites. Table 3 and Table 4 give the mechanical properties of the carbon fiber and glass fiber composites, respectively.

Table 2. Aluminum temperature dependent material properties (elastic model).

Temperature (°C)	**-75**	**25**	**100**	**150**	**200**
Density (kg/m^3)[1, 2]	2,700	2,700	2,700	2,700	2,700
E (GPa)	72.0	69.0	66.0	63.0	60.0
ν[1]	0.33	0.33	0.33	0.33	0.33

[1] Temperature dependent values were not given by Table PRD of the ASME BPVC.
[2] For implicit quasistatic analyses, Sierra requires the specification of an arbitrary value for density for material models. Therefore, a constant value for the density has not effect on the solution.

Table 3. Carbon fiber composite temperature dependent material properties (elastic orthotropic model).

Temperature (°C)	**-54**	**25**	**71**	**160**
Density (kg/m^3)[1]	1,600	1,600	1,600	1,600
E_{11} (GPa)	63.86	63.86	63.86	63.86
E_{22} (GPa)	62.74	62.74	62.74	62.74
E_{33} (GPa)	12.17	8.59	6.50	2.462
ν_{12}	0.048	0.048	0.048	0.048
ν_{13}	0.408	0.408	0.408	0.408
ν_{23}	0.408	0.408	0.408	0.408
G_{12} (GPa)	4.87	3.44	2.60	0.99
G_{13} (GPa)	4.63	3.27	2.47	0.94
G_{23} (GPa)	4.61	3.25	2.46	0.93

[1] For implicit quasistatic analyses, Sierra A requires the specification of an arbitrary value for density for material models. Therefore, a constant value for the density has not effect on the solution.

Table 4. Glass fiber composite temperature dependent material properties (elastic orthotropic model).

Temperature (°C)	**-54**	**25**	**71**	**160**
Density (kg/m^3)[1]	1,600	1,600	1,600	1,600
E_{11} (GPa)	28.55	24.75	22.54	18.27
E_{22} (GPa)	26.54	23.10	21.09	17.21
E_{33} (GPa)	14.56	9.72	6.91	1.46
ν_{12}	0.152	0.130	0.117	0.092
ν_{13}	0.36	0.36	0.36	0.36
ν_{23}	0.36	0.36	0.36	0.36
G_{12} (GPa)	5.16	3.45	2.45	0.52
G_{13} (GPa)	4.40	2.94	2.09	0.44
G_{23} (GPa)	4.40	2.94	2.09	0.44

[1] For implicit quasistatic analyses, Sierra Adagio requires the specification of an arbitrary value for density for material models. Therefore, a constant value for the density has not effect on the solution.

Temperature dependent CTEs for aluminum were found in Table TE-2 of the ASME BPVC gives average CTEs for the temperature ranges 20 °C to 100 °C and 20 °C to 200 °C [11]. Using these CTEs (Table 5), thermal strains were calculated at -50 °C, 100 °C, and 200 °C and supplied to Sierra Adagio using a piecewise linear function.

The CTEs of the cured composites were measured over the temperature range -50 °C to 150 °C in 10 °C increments, as shown in Figure 7 and given in

Table 6 and Table 7 for carbon fiber and glass fiber composites, respectively. Thermal strains were calculated at each increment and supplied to Sierra Adagio using a piecewise linear function.

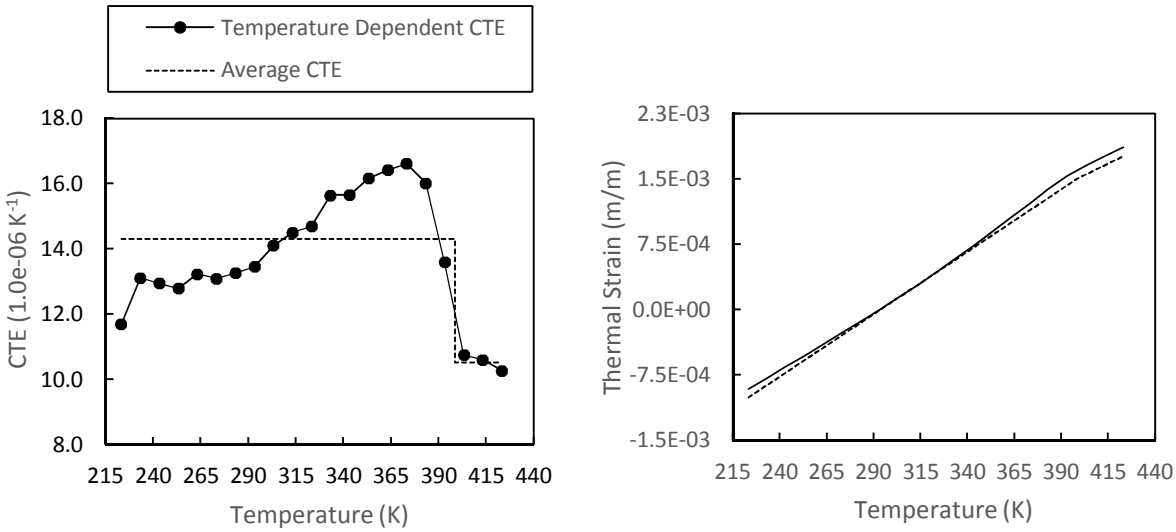

Figure 7. Comparison of temperature dependent and average CTE (left) and corresponding thermal strains (right) for the glass fiber composite CTE_{11}.

Table 5. Temperature dependent CTEs (1.0e-06 K^{-1}) for aluminum.

Temperature (°C)	**20**	**30**	**40**	**50**	**60**	**70**	**80**	**90**	**100**	**110**	**120**	**130**	**140**	**150**
All directions	23.4	23.4	23.4	23.4	23.4	23.4	23.4	23.4	25.4	25.4	25.4	25.4	25.4	25.4

Table 6. Temperature dependent CTEs (1.0e-06 K^{-1}) for the carbon fiber composite.

Temperature (°C)	20	30	40	50	60	70	80	90	100	110	120	130	140	150
11 direction	2.9	2.8	2.9	3.2	3.4	3.6	3.9	4.1	3.9	3.6	1.9	1.0	1.0	2.0
22 direction	3.2	3.3	3.3	3.6	3.7	3.9	4.0	4.2	4.4	4.4	3.3	2.8	2.1	2.2
33 direction	55.6	57.4	61.3	64.2	68.9	73.7	79.2	87.0	100.3	130.0	190.1	226.6	227.6	231.3

Table 7. Temperature dependent CTEs (1.0e-06 K^{-1}) for the glass fiber composite.

Temperature (°C)	20	30	40	50	60	70	80	90	100	110	120	130	140	150
11 direction	13.5	14.1	14.5	14.7	15.6	15.7	16.2	16.4	16.6	16.0	13.6	10.7	10.6	10.3
22 direction	13.9	14.3	14.6	15.5	15.7	16.0	17.0	17.3	17.8	18.0	17.2	14.6	11.9	10.2
33 direction	46.3	48.5	51.8	55.6	59.3	64.0	69.8	78.8	94.3	128.7	184.9	241.6	255.5	262.8

3.4.4 Temperature Independent Properties

The temperature independent mechanical properties for the aluminum and cured composites were specified using the room temperature (25 °C) values previously specified.

The thermal strains for aluminum were specified using the average CTE from the temperature range 20 °C to 100 °C, which is 23.4e-06 K^{-1}.

The thermal strains for the composite materials were not truly temperature independent as the CTEs were differentiated by the glassy and rubbery regions of the composite. For both the carbon fiber and glass fiber composites, the glass transition temperature (T_g) was set at 125.1 °C. For the temperature independent model, the thermal strains for the composites were calculated based on average CTEs for temperatures below and above T_g.

Table 8. Average CTEs (1.0e-06 K^{-1}) for the carbon fiber composite.

Temperature (°C)	$< T_g$ [1]	$> T_g$
11 direction	3.15	0.95
22 direction	3.62	2.18
33 direction	67.6	228.5

[1] Average CTEs below T_g were averaged over all temperatures sampled in the glassy region (-50 ° to T_g)

Table 9. Average CTEs (1.0e-06 K^{-1}) for the glass fiber composite.

Temperature (°C)	$< T_g$ [1]	$> T_g$
11 direction	14.32	10.54
22 direction	15.08	12.26
33 direction	58.92	253.30

[1] Average CTEs below T_g were averaged over all temperatures sampled in the glassy region (-50 ° to T_g)

3.5 Model Geometry

The geometry of the split ring was generated and meshed in three-dimensions using Cubit using the nominal inner diameter of the aluminum (108.2 mm) and the average aluminum and total thicknesses (1.91 mm / 1.86 mm and 3.46 mm / 3.34 mm, respectively (carbon fiber / glass fiber)). The small dimensional variances in the thicknesses are negligible with regards to the final residual stress state of the split ring. Additionally, since the material model for the composites was specified with homogenous properties within the elastic orthotropic model, the composite layer was modeled as one section instead of individual plies.

The split ring was modeled in quarter symmetry with a width of 12.7 mm as a complete cylinder. While the split ring was manufactured as part of a larger cylinder, the aluminum was expected to remain elastic and, therefore, modeling the split ring at its final width is acceptable. A partition for the sector that would be removed in the third simulation step was made as well as a partition for the scribe lines used in the subsequent testing. Symmetry was specified on the xy and yz planes and a single node along the cut surface was held at zero y-displacement to prevent any motion (Figure 8).

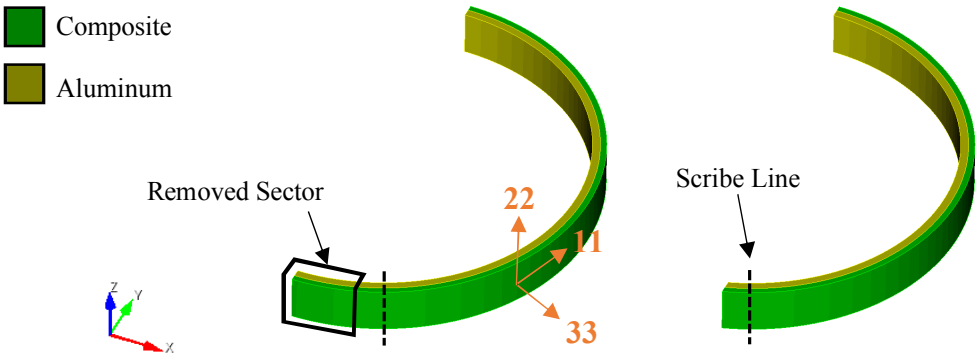

Figure 8. Bi-material split ring simulation geometry before (left) and after (right) sector removal.

The composite material was orientated in cylindrical coordinates such that the 11 direction was aligned with the circumference and the 22 direction was parallel to the split ring's axis for the glass fiber simulation and one of the carbon fiber simulations. The remaining carbon fiber simulation rotated the composite material 45° about the 33 direction.

Based on the fiber orientation for the bi-material split ring with the carbon fiber composite skewed 45°, symmetry should not be used. However, since the mechanical and thermal properties in the 11 and 22 directions are similar, symmetry is an acceptable assumption for composites with 45° skew.

3.6 Mesh Convergence Study

Each model underwent a mesh convergence study in order to verify that the model solution was converging to the same continuum value (maximum displacement for the plate and gap width for the cylinder) regardless of mesh. Additionally, the mesh convergence study aids in determining a balance between computational efficiency and solution error.

The mesh convergence studies followed Richardson's Extrapolation [12]. By using Richardson's Extrapolation, an estimate of the exact value, or the solution corresponding to an element size of zero, can be determined from the solutions to three uniformly refined meshes. The three meshes, shown in Figure 9, begin with one element through the thickness of the aluminum and composite layers and increase to two and four for the subsequent meshes. Table 10 and Table 11 show the scribe line widths for each of the meshes, the estimated continuum solution, and the mesh error for each of the bi-material split rings. In order to minimize error relating to the mesh (to ~1 % or less), the most refined mesh (four elements through the thickness) was used to compare with the experimental results as it was still computationally inexpensive.

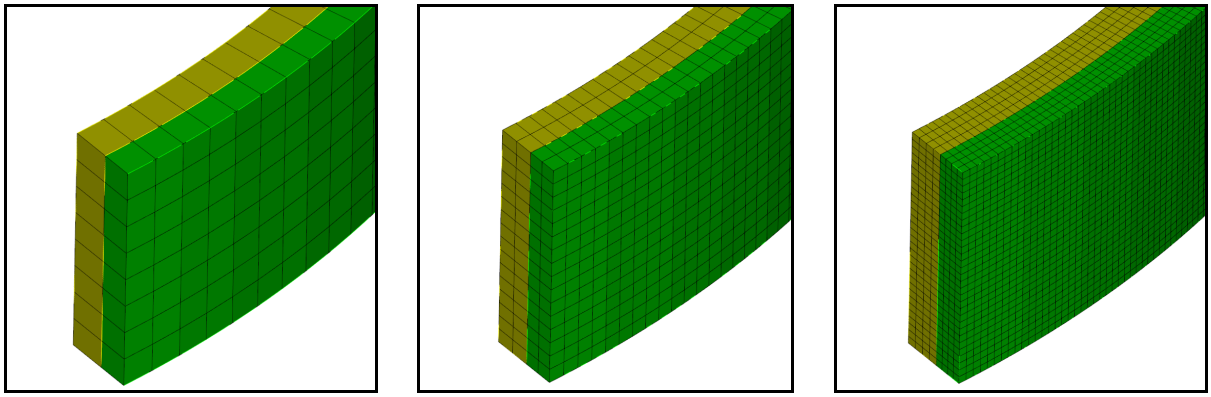

Figure 9. Bi-material split ring simulation geometry before (left) and after (right) sector removal.

Table 10. Mesh convergence results for the carbon fiber composite split rings.

Mesh	Element Size (mm)	Total Elements	No Skew		45° Skew	
			Scribe Line Width (mm)	Error	Scribe Line Width (mm)	Error
1	1.63	1,744	17.20	22.9 %	21.86	24.5 %
2	0.81	13,824	21.28	4.6 %	27.50	5.1 %
3	0.41	107,136	22.10	0.9 %	28.67	1.1 %
Exact	-	-	22.30	-	28.97	-

Table 11. Mesh convergence results for the glass fiber composite split rings.

Mesh	Element Size (mm)	Total Elements	No Skew	
			Scribe Line Width (mm)	Error
1	1.51	2,196	37.63	8.4 %
2	0.76	16,320	40.44	1.5 %
3	0.38	133,840	40.95	0.3 %
Exact	-	-	41.07	-

4. RESULTS

Similar to the experiment, the simulated split ring was heated from 20 °C to 150 °C and the width of the scribe lines was monitored. Figure 10 through Figure 12 compare the temperature independent and dependent models to the experiments.

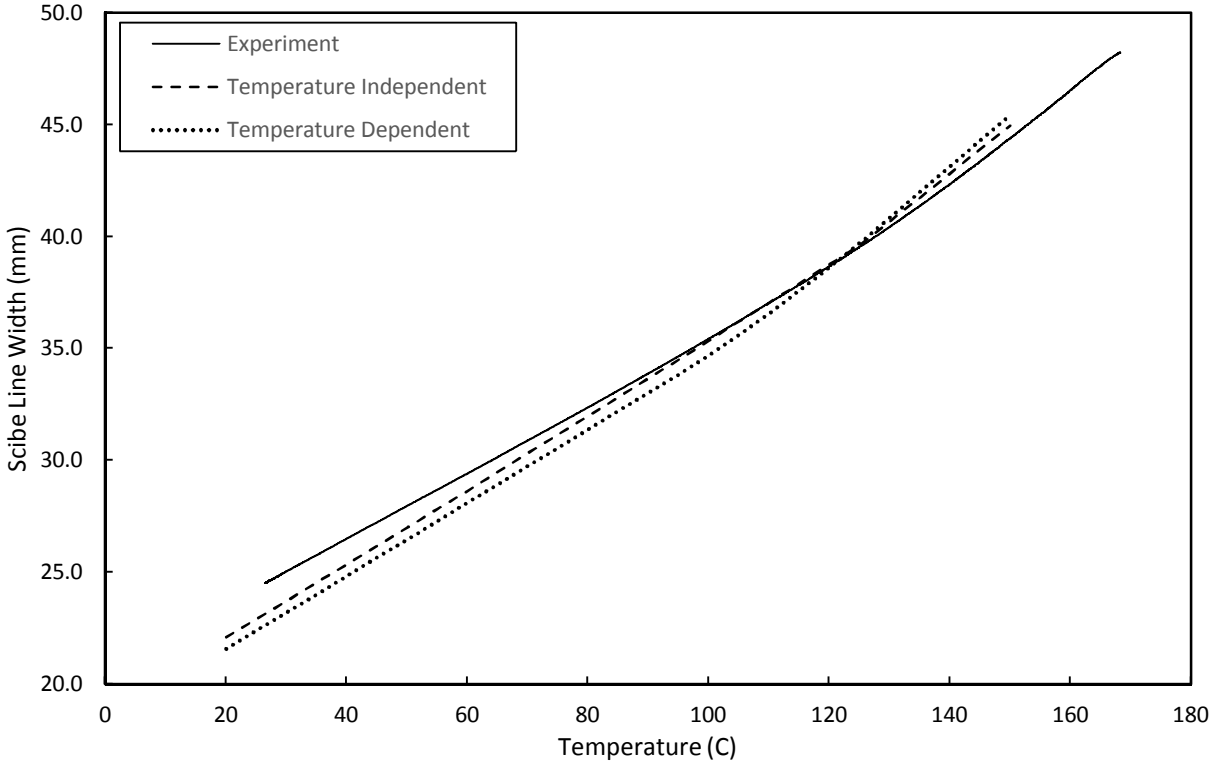

Figure 10. Scribe line width as a function of temerature: Aluminum/Carbon Fiber Composite (no skew).

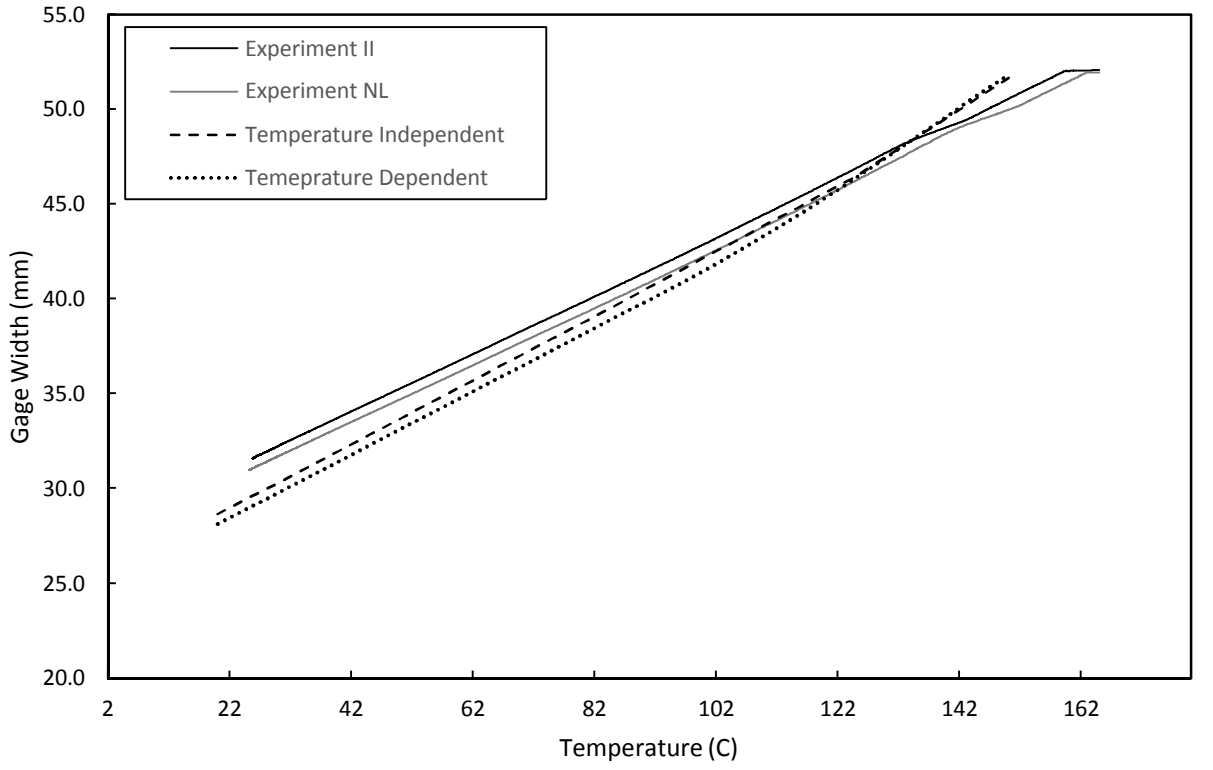

Figure 11. Scribe line width as a function of temerature: Aluminum/Carbon Fiber Composite (45° skew).

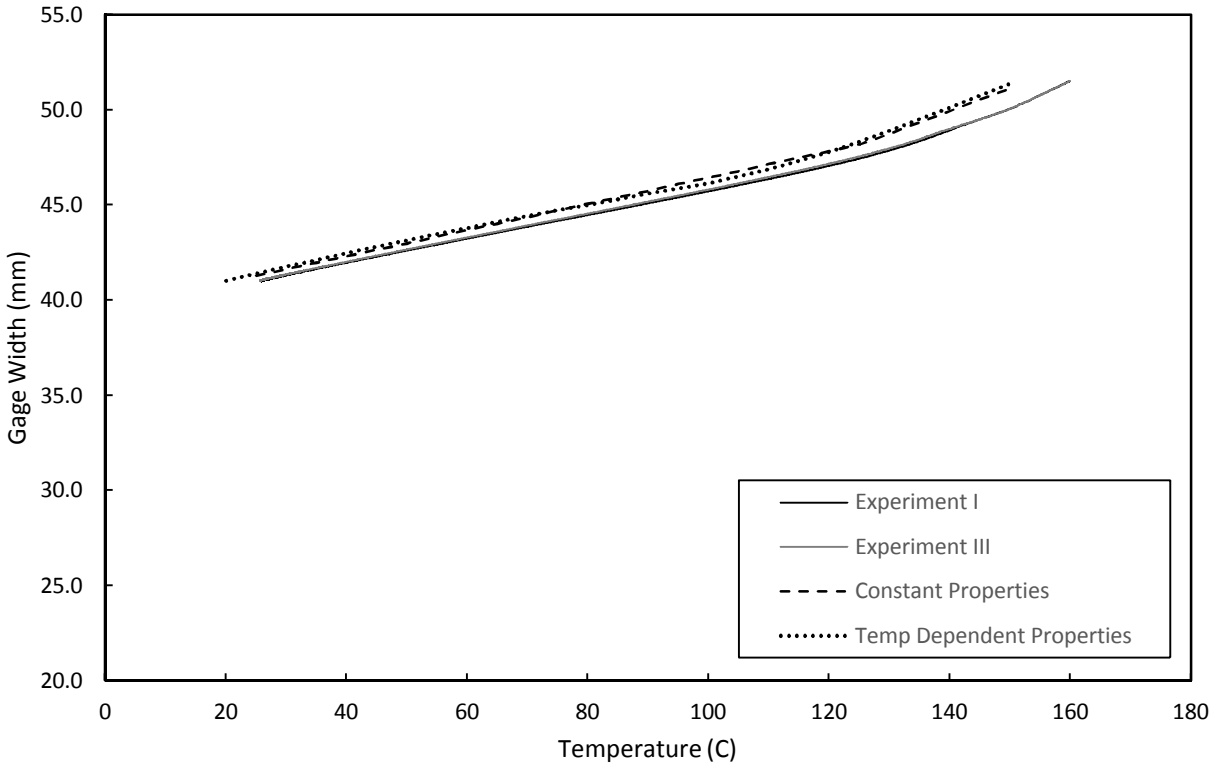

Figure 12. Scribe line width as a function of temerature: Aluminum/Glass Fiber Composite (no skew).

5. CONCLUSIONS

A simplified composite process modeling methodology was used to predict the residual stresses due to the composite curing process in split rings with different composites and orientations, which were then compared to experimentally determined displacements over a range of temperatures. The simulation methodology showed good agreement with the experiments for all materials and orientations, as well as for both the temperature independent and dependent material models. For temperatures below the glass transition temperature, the simulation shows better agreement with the experiments than temperatures greater than T_g. From this, it can be concluded that extrapolating the temperature dependence into the rubbery region of the composite from experimental results solely in the glassy region is not sufficient to capture the behavior within the rubbery region. Furthermore, the temperature independent and dependent models remain within a few percent error of each other over the entire simulation – in both the glassy and rubbery region of the composites. This indicates that a temperature independent model is sufficient in predicting the residual stress state of the bi-material split rings with a reasonable level of accuracy compared to the temperature dependent model. This also suggests that changing the behavior of the composite's mechanical properties to be similar to that of the coefficients of thermal expansion of the temperature independent material model (partially temperature dependent with a single value for above and below T_g) may improve the results in the rubbery region of the composite. However, these material properties should be experimentally determined and not extrapolated from lower temperature experiments.

6. ACKNOWLEDGEMENTS

The authors are grateful to Helena Jin of Sandia National Laboratories for conducting the necessary experiments to determine the temperature dependence of the mechanical properties for the composite materials used in this investigation.

7. REFERENCES

1. Timoshenko S. "Analysis of bi-metal thermostats." *Journal of the Optical Society of America* 11(1925):233-255.
2. Jumbo, F.S., Ashcroft, I.A., Crocombe, A.D., and Abdel Wahab, M.M. "Thermal residual stress analysis of epoxy bi-material laminates and bonded joints." *International Journal of Adhesion & Adhesives* 30(2010):523-538.
3. White, S.R., Hahn, H.T. "Process Modeling of Composite Materials: Residual Stress Development during Cure. Part I. Model Formulation." *Journal of Composite Materials* 26(1992):2402-2422
4. White, S.R., Hahn, H.T. "Process Modeling of Composite Materials: Residual Stress Development during Cure. Part II. Experimental Validation." *Journal of Composite Materials* 26(1992):2423-2453
5. Tavakol, B., Roozbehjavan, R., Ahmed, A., Das, R., Joven, R.M Koushyar, H., Rodriguez, A., Minaie, B. "Prediction of Residual Stresses and Distortion in Carbon Fiber-Epoxy Composite Parts Due to Curing Process Using Finite Element Analysis." *Journal of Applied Polymer Science* (2013):941-950
6. Volk, B.L., Braginsky, M., Hoos, K., Iarve, E., Mollenhauer, D., and Storage, T. "Predicting the open hole tension of organic matrix composites incorporating the effects of processing." *CAMX Conference Proceedings.* Dallas, TX, October 26-29, 2015. *CAMX – The Composites and Advanced Materials Expo* CD-ROM
7. Volk, B.L., Nelson, S.M., Hanson, A.A., Briggs, T.M., Storage, T., and Werner, B.T. "Evaluation of Process Modeling methodologies for Out-of-Autoclave Polymer Matrix Composites." *CAMX Conference Proceedings.* Anaheim, CA, September 26-29, 2016. *CAMX – The Composites and Advanced Materials Expo* CD-ROM
8. Hanson, A.A., Nelson, S.M., Briggs, T.M., Werner, B.T., Volk, B.L., and Storage, T. "Experimental Measurement and Finite Element Modeling of Residual Stresses in Simple Composite Structures." *CAMX Conference Proceedings.* Anaheim, CA, September 26-29, 2016. *CAMX – The Composites and Advanced Materials Expo* CD-ROM
9. Hahn, H.T. "Residual Stresses in Polymer Matrix Composite Laminates." *Journal of Composite Materials* 10(1976):266-278
10. SIERRA SolidMechanics Team (2017). *SIERRA/SolidMechanics 4.44 User's Guide*, Sandia National Laboratories, Albuquerque, NM.
11. AMSE Boiler & Pressure Vessel Code Section II Part D, 2015.
12. Roache, P.J. "Perspective: A Method for Uniform Reporting of Grid Refinement Studies." *Journal of Fluids Engineering* 116(1994):405-413